α_{eI} = combination of variables used in Table 3 $(Q\Delta C_{pi}R_c^2/K_e)$
α_{eII} = combination of variables used in Table 3 $(Q\Delta C_{pII}R_c^2/K_e)$
ΔC_{pI} = combination of C_{pi}'s
ΔC_{pII} = combination of C_{pi}'s
ΔH_c = enthalpy change for the reaction $C + O_2 \rightarrow CO_2$
ΔH_w = enthalpy change for the reaction $H_2 + \frac{1}{2}O_2 \rightarrow H_2O$
ΔH_I = enthalpy change for the reaction $C + 2H_2O \rightarrow CO_2 + 2H_2$
ϵ = ash layer porosity
ρ_{CF} = mass of fixed carbon per unit unreacted particle volume conditions

Subscript

B = condition in the bulk phase
c = condition at the core surface

Superscript

c = condition at the core surface

LITERATURE CITED

Arthur, J. R., "Reactions Between Carbon and Oxygen," *Trans. Faraday Soc.*, **47**, 164 (1951).

Burke, S. P., and T. E. W. Schumam, "The Mechanism of Combustion of Solid Fuel," *Proc. 3rd Intern. Conf. Bituminous Coal*, **2**, 485 (1931).

Blackwood, J. D., "The Kinetics of the System Carbon-Hydrogen-Methane," *Aust. J. Chem.*, **15**, 397 (1962).

———, and D. J. McCarthy, "The Mechanism of Hydrogenation of Coal to Methane," *ibid.*, **19**, 797 (1966).

Blackwood, J. D., and F. McGrory, "The Carbon-Steam Reaction at High Pressure," *ibid.*, **11**, 16 (1958).

Caram, H., and N. R. Amundson, "Diffusion and Reaction in a Stagnant Boundary Layer About a Carbon Particle," *Ind. Eng. Chem. Fundamentals*, **16**, No. 2, 171 (1977).

Gibson, M. A., and C. A. Euker, Jr., "Mathematical Modeling of Fluidized Bed Coal Gasification," preprint presented at AIChE Symposium on Laboratory Reactors, Los Angeles, Calif. (Nov., 1975).

Field, M. A., D. W. Gill, B. B. Morgan, and P. G. W. Hawksley, "Combustion of Pulverized Coal," The British Coal Utilization Research Association, Leatherhead (1967).

Institute of Gas Technology, "Production of Pipeline Gas by Hydrogasification of Coal," *Res. Bull. No. 39*, 1 (1972).

Johnson, J. L., "Kinetics of Bituminous Coal Char Gasification with Gases Containing Steam and Hydrogen," *Adv. Chem. Ser.*, 131, ACS (1974).

Spalding, D. B., *Some Fundamentals of Combustion*, Butterworths, London, England (1955).

van der Held, E. F. M., "The Reaction Between a Surface of Solid Carbon and Oxygen," *Chem. Eng. Sci.*, **14**, 300 (1961).

Wen, C. Y. and S. C. Wang, "Thermal and Diffusional Effects in Non-Catalytic Solid Gas Reactions," *Ind. Eng. Chem.*, **62**, No. 8, 30 (1970).

Wen, C. Y., and J. Huebler, "Kinetic Study of Coal Char Hydrogasification. Rapid Initial Rate," *Ind. Eng. Chem. Process Design Develop.*, **4**, 142 (1965).

———, "Kinetic Study of Coal Char Hydrogasification. Second-Phase Reaction," *ibid.*, 147 (1965).

Wicke, E., and G. Wurzbacher, "Konzentrationsprofile vor einer im Sauerstoffstrom verbrennenden hohlenstoffoberfläche I.," *Intern. J. Heat Mass Transfer*, **5**, 277 (1962).

Manuscript received May 13, 1977; revision received and accepted August 23, 1977.

Char Gasification in a Countercurrent Reactor

NEAL R. AMUNDSON
and
LUIS ERNESTO ARRI

Department of Chemical Engineering and Materials Science
University of Minnesota
Minneapolis, Minnesota 55455

A model is developed for the countercurrent char gasifier of Lurgi form. Char particles are fed to the top and oxygen, inert, and steam in the bottom. The combustion zone is defined as the zone in which there is a nonzero molfraction of oxygen. In the gasification zone, the particles are assumed to be a lumped system in which the Johnson reaction kinetic expressions are assumed to be valid with the water gas shift reaction at equilibrium. All of the reactions between oxygen and carbon and water and carbon are assumed to take place in the combustion zone but with the carbon-oxygen reaction predominating to form a shell progressive system within the particles. Radiation is taken into account, and parametric computations are made on temperatures, compositions, flow rates, and char reactivity. The maximum temperature is strongly influenced by radiation and its position is a sensitive function of the solid flow rate producing an ash layer at the bottom of varying thickness.

SCOPE

The purpose of this study was to develop a model for a countercurrent moving-bed gasifier of coal, actually char, which would predict at least qualitatively the known features of such systems. There has been little modeling with this system, although the general subject of gas-solid reactions in moving beds has been examined in detail, notably by Ishida and Wen (1971) and Wen and Wang (1970). A quantitative model of the countercurrent gasifier was presented by Yoon et al. (1976), and there have been numerous descriptive and qualitative discussions by Elgin and Perks (1973, 1974), Rudolph (1974), Hebden (1975), and Hoogendorn (1973). In addition, Woodmansee (1975) updated some very early models. There is almost no real operating information available in the literature, and one

Neal R. Amundson is at the University of Houston, Houston, Texas 77004. Luis Ernesto Arri is with INTEC (U.N.L-CONICET), Santiago del Estero 2654, 3000 Santa Fé, Argentina.

must test his model against the described qualitative behavior in many cases. The model studied assumes that in the upper gasification zone, the three reactions used by Johnson (1974) in his studies of gasification reaction kinetics take place, coupled with the appropriate transport equations. In the combustion zone, where there is oxygen present, the particles are assumed to follow a shell progressive model determined largely by the carbon-oxygen reaction. Within the core, the gasification reactions occur, but because of the presence of oxygen only carbon dioxide emerges. The model takes into consideration radiation from particle to particle. Parametric studies are made in some of the pertinent parameters. While the model is conceptually simple and at the same time relatively realistic, there were some severe computational problems which had to be overcome. These are not discussed.

CONCLUSIONS AND SIGNIFICANCE

Parametric studies were made to show the effect of some of the basic parameters of the system such as oxygen/steam mole ratio in the feed, solids flow rate, and temperatures. It was shown that radiation had a marked effect on the operation since its presence resulted in substantially lower maximum temperatures in the bed than by neglecting it. This is important, since the ash fusion temperature must be avoided. One of the remarkable results obtained, and one which is known to be a difficulty in operation, is the location of the maximum temperature and its relation to the thickness of the ash layer at the bottom of the reactor. If there is residual carbon coming out of the bottom, the maximum temperature occurs at the bottom. On the other hand, if there is an ash layer, its thickness is a strong function of the solid flow rate so that the position of maximum temperature could wander in the bed because of the difficulty in maintaining a steady solids flow rate.

In an earlier paper, a single char particle exposed to a constant environment was considered in some detail. The purpose of that analysis was to obtain a better understanding of what occurred under certain hypothetical conditions. The purpose of this paper is to construct what is hoped is a reasonable model for a countercurrent gasifier in which coal is fed to the top of a moving-bed reactor and oxygen, steam, and perhaps inert material at the bottom. It is well known that coal devolatilization is a fairly rapid process proceeding without major heat effect. The oxygen mixture fed into the bottom will eventually, as it proceeds upwards, reach a high enough temperature so that the reaction between carbon and oxygen will commence, and this reaction will proceed upwards until all or almost all of the oxygen is consumed. The reaction mixture at this point consists of water, carbon dioxide, and inert. More will be said about this later. Since the oxygen is exhausted, the reactions willl now be between carbon, carbon dioxide, water, and hydrogen. We will be interested in the development of a model and will make appropriate parametric studies. It is unfortunate that in spite of the operation of such reactors since 1936 in Germany, there is almost no quantitative information in the literature; however, the paper of Hebden (1975) should be mentioned, and qualitative agreement is established.

While there has been substantial research on reactors for solid-gas reactions, we will mention only those concerned with the combustion of carbon in countercurrent moving bed reactors. Woodmanasee (1975) updated some earlier models. These models assume equilibria among the reactions and include some simplifying assumptions in the energy conservation equations, many of which may be invalid. Recently, Yoon, Wei, and Denn (1976) presented a paper in which a shell progressive model was used with somewhat different reactions and assumptions on the heat transfer than those made here. It is strange that with the worldwide interest in the Lurgi reactor there has been so little in the way of modeling or on design equations presented.

In this paper we will assume, as mentioned above, that char is fed to the top of the reactor and an oxygen-water vapor-inert mixture at the bottom. The lower zone, referred to in the future as the combustion zone, extends from the bottom of the reactor to the point where oxygen has been completely exhausted. The reactions in the combustion zone are

$$C + \tfrac{1}{2} O_2 \rightarrow CO \qquad (1)$$

$$H_2 + \tfrac{1}{2} O_2 \rightarrow H_2O \qquad (2)$$

$$CO + \tfrac{1}{2} O_2 \rightarrow CO_2 \qquad (3)$$

$$CO + H_2O \rightarrow CO_2 + H_2 \qquad (4)$$

We assume there is no methane formation in this zone. Reactions (2) and (3) are very fast and proceed to completion, and reaction (4) is fast and proceeds to a finite equilibrium. Reaction (1) is responsible for our assumption of the shell progressive model. In the upper zone there is no oxygen, and so the reactions taking place here are

$$CO_2 + C \rightarrow 2CO \qquad (5)$$

$$H_2O + C \rightarrow CO + H_2 \qquad (6)$$

$$2H_2 + C \rightarrow CH_4 \qquad (7)$$

$$CO + H_2O \rightarrow CO_2 + H_2 \qquad (8)$$

The first three reactions are relatively slow.

Let us now hypothesize about the model. The carbon spheres as they descend from the top contact carbon dioxide, carbon monoxide, hydrogen, and water. Since the reactions with carbon are slow, we assume that diffusion plays no role, so that the concentrations of the various species will be uniform throughout the particle. If one assumes that the water gas shift reaction is very fast and always at equilibrium, the concentration of hydrogen, carbon monoxide, carbon dioxide, and water are related throughout the gasification zone by the equilibrium relationship.

When the particles enter the combustion zone from the gasification zone, they come into contact with oxygen for the first time, and the homogeneous spherical particle develops a spherical core of radius R_c, where $R_c < R_p$, and the core is surrounded by a shell like ash layer through which the reactants must diffuse to reach the core surface. Oxygen will react at the core surface, and in the core hydrogen, carbon monoxide, and carbon dioxide will be formed. However, the hydrogen and carbon monoxide

formed will diffuse outward to the core surface and will be consumed by oxygen. Thus, all of the hydrogen produced from the water returns to water, and all of the carbon monoxide produced reacts at the core surface to produce carbon dioxide. Thus, on the assumption that there is sufficient oxygen, the only diffusing reactants through the ash layer are oxygen into the particle and carbon dioxide from the particle. Now, as shown in the single-particle studies, there may be insufficient oxygen in the interstitial gas to do all of this. Under these conditions some of the carbon monoxide and hydrogen will diffuse into the ash layer, meet the oncoming oxygen and react, thus forming, on the assumption of instantaneous reaction, a flame front. Under these conditions, if a shrinking core has already been formed, its size would become fixed. The amount of carbon in it would be reduced uniformly, and the flame front would be established either in the ash layer or, with a similar argument, in the boundary layer surrounding the particle. This makes the problem very difficult to model, since there is a core in the combustion zone, there is plenty of oxygen at the bottom of the reactor, but near the end of the combustion zone the flame front may not be at the core surface.

The object of our model is to predict the gas composition from the reactor, the temperature distribution, and the maximum temperature. In the practical operation of the Lurgi reactor it is known that the control of the position of the hot spot is very difficult. This comes out in this work as an obvious consequence of the fact that the thickness of the ash layer at the bottom of the reactor, assuming that all of the carbon can be consumed, may be a very sensitive function of the solid flow rate in the reactor. In our treatment here we will depend heavily on the previous single-particle studies and will not repeat what was given there. The expressions for the reaction rates of the various reactions will be the same as in that paper.

DEVELOPMENT OF EQUATIONS FOR COMBUSTION ZONE

In the previous paper, the authors (1977) developed equations that relate the internal concentrations and temperature fields (x^c_{H2O}, x^c_{O2}, T_c) to the external parameters ($x_{O2,B}$, T_B). In that development, the pseudo steady state approximation was used which may not be realistic for energy balances. To avoid dealing with the system of partial differential equations which would result from the shrinking core model when the pseudo steady state assumption is relaxed, an approximate method that yields a simplified heat balance (Beverage and Goldie, 1968; Wen and Wang 1970; Ishida and Wen, 1971) will be used, adapted to our treatment.

In the studies on the single particle, the authors postulated a shell progressive mechanism determined primarily by the reaction $C + \frac{1}{2} O_2 \rightarrow CO$ at the core surface, while in the core of the particle the gasification of carbon with carbon dioxide and steam together with the water gas shift reaction take place. Very fast reactions between gasification products (carbon monoxide and hydrogen) and oxygen are assumed, and the existence of a flame front either at the core surface or outside it is possible. From outside such a flame front, the whole process can be visualized as a simple reaction $C + O_2 \rightarrow CO_2$ with the outer region under a simple oxygen-carbon dioxide equimolar countercurrent diffusion. If the oxygen concentration in the bulk phase is too low (or the core temperature too high), the flame front will not occur at the core surface as it might with higher values but will pull away from the core surface, and all of the oxygen will be exhausted either in the ash layer, if it has already been formed, or in the boundary layer by reaction with hydrogen and carbon monoxide produced in the core of the particle. By solving the oxygen conservation equations, the oxygen molar flux at the outer edge of the boundary layer can be computed to be

$$N_{O2}|_{r=R_\delta} = \begin{cases} -(Q_{H2O} + K_1 x^c_{O2})\left(\frac{R_c}{R_\delta}\right)^2; & R^* = R_c \\ -Q_{H2O}\left(\frac{R_c}{R_\delta}\right)^2 ; & R_c < R^* \leq R_p \\ -Q_{H2O}\left(\frac{R_c}{R_\delta}\right)^2 ; & R_p < R^* \leq R_\delta \end{cases}$$

which can be summarized by

$$N_{O2}|_{r=R_\delta} = -Q\left(\frac{R_c}{R_\delta}\right)^2$$

where the expression for Q, the total rate of carbon consumption for each of the three possible situations, can be immediately obtained by direct inspection. The oxygen mole fraction at the core surface was found to be given by

$$x^c_{O2} = \frac{x_{O2,B} - \frac{Q_{H2O}R_c^2}{cD}\left[\left(\frac{1}{R_p} - \frac{1}{R_\delta}\right) + \frac{1}{\epsilon^2}\left(\frac{1}{R_c} - \frac{1}{R_p}\right)\right]}{1 + \frac{k_1 R_c^2}{cD}\left[\left(\frac{1}{R_p} - \frac{1}{R_\delta}\right) + \frac{1}{\epsilon^2}\left(\frac{1}{R_c} - \frac{1}{R_p}\right)\right]}$$

if the flame front is at the core and zero otherwise.

On performing a shell balance for each of the gaseous species in a differential element of volume of the reactor in the combustion zone, we get

$$\frac{d(Gg_i)}{dx} = \left(\frac{R_\delta}{R_p}\right)^2 aN_i$$

for all i. Since

$$\Sigma g_i M_i = \Sigma w_i = 1$$

multiplying each of the species mass balances by the corresponding molecular weight and adding, we can compute the rate of change of the total mass flow rate of the gas phase along the combustion zone to be

$$\frac{dG}{dx} = M_c\, aQ\left(\frac{R_c}{R_p}\right)^2$$

The mass balance for oxygen, which is taken to be the independent component, can then be written

$$\frac{dg_{O2}}{dx} = -\frac{(1 + M_c g_{O2})^2\, aQ(R_c/R_p)^2}{G^o(1 + M_c g^o_{O2})}$$

The concentrations of all the other species and the total mass flow rate for the gas phase can be computed in terms of the oxygen concentration and feed data to give

$$G = \frac{G^o(1 + M_c g^o_{O2})}{1 + M_c g_{O2}}$$

$$g_{H2O} = \frac{(1 + M_c g_{O2}) g^o_{H2O}}{1 + M_c g^o_{O2}}$$

$$g_{N2} = \frac{(1 + M_c g_{O2}) g^o_{N2}}{1 + M_c g^o_{O2}}$$

$$g_{CO2} = \frac{1 + M_c g_{O2}}{1 + M_c g^o_{O2}}(g^o_{O2} + g^o_{CO2}) - g_{O2}$$

In moving down the reactor, the core of the char particle will suffer changes in its radius and in its conversion which are given by

$$\frac{dR_c}{dx} = \frac{a\,R_p M_c R_1}{3R_{SF}(1-w_{AF})(1-X)}$$

$$\frac{dX}{dx} = \frac{M_c Q_{H2O}\,a\,R_p}{R_c(1-w_{AF})F_{SF}}$$

respectively.

The method used to obtain the heat balance for the solid phase in the combustion zone can be summarized as follows. 1. An average temperature (T_{av}) for the ash layer is defined and an energy balance for the solid phase is written for a differential element of volume of the bed. A functional relation among the accumulation in the core (dT_c/dx), the accumulation in the ash layer (dT_{av}/dx), and the radiation flux $\left[\frac{d}{dx}\left(K_R \frac{dT_{PS}}{dx}\right)\right]$ is obtained. 2. A pseudo steady state profile for the ash layer is assumed in terms of the core temperature (T_c) and the temperature of the external surface of the particle (T_{PS}). Such an assumed profile allows us to compute T_{av}. 3. A relation between T_{PS} and T_c is established, since all of the heat conducted through the ash layer should be dissipated at the external surface of the particle either by conduction through the boundary layer or by radiation to the surrounding layers of particles.

An energy balance for the solid phase for an element of volume in the bed can be written as

$$\frac{F_{SF}}{\frac{4}{3}\pi R_p^3 \rho_{SF}}\left[\int_0^{R_p}(\rho_a\tilde{h}_a+\rho_c\tilde{h}_c)4\pi r^2 dr\,\Big|_{x+\Delta x} - \int_0^{R_p}(\rho_a\tilde{h}_a+\rho_c\tilde{h}_c)4\pi r^2 dr\,\Big|_{x}\right] - \left\{-K\frac{\partial T}{\partial r}\Big|_{r=R_p} + \sum_i N_i h_i\Big|_{r=R_p}\right\} a\,\Delta x + K_R\frac{dT_{PS}}{dx}\Big|_{x+\Delta x} - K_R\frac{dT_{PS}}{dx}\Big|_{x} = 0 \quad (1)$$

where the radiation flux has been taken into account by means of an apparent axial conductivity. If we call

$$I = \int_0^{R_p}(\rho_a\tilde{h}_a+\rho_c\tilde{h}_c)r^2 dr$$

Equation (1) can be written in differential form as

$$\frac{3F_{SF}}{\rho_{SF}R_p^3}\frac{dI}{dx} = -\frac{d}{dx}\left(K_R\frac{dT_{PS}}{dx}\right) + \left\{-K\frac{\partial T}{\partial r} + \Sigma N_i h_i\right\}\Big|_{r=R_p^+} a \quad (2)$$

As the integrand of I is discontinuous at $r = R_c$, and because the discontinuity surface is moving, differentiating I after rearrangement we get

$$\frac{dI}{dx} = \tilde{h}_c\Big|_{r=R_c^-}\frac{R_c^3}{3}\frac{d\rho_c}{dx} + (\rho_c\tilde{C}_{pc}+\rho_a\tilde{C}_{pa})\Big|_{r=R_c^-}\frac{R_c^3}{3}\frac{dT_c}{dx} + \tilde{h}_c\rho_c|_{r=R_c^-}R_c^2\frac{dR_c}{dx} + \rho_a\tilde{C}_{pa}\int_{R_c}^{R_p}\frac{\partial T}{dx}r^2 dr \quad (3)$$

If we define the average ash layer temperature to be

$$T_{av} = \frac{\int_{R_c}^{R_p} r^2 T\,dr}{\int_{R_c}^{R_p} r^2 dr}$$

it can be shown that

$$\int_{R_c}^{R_p}\frac{\partial T}{\partial x}r^2 dr = \frac{R_p^3-R_c^3}{3}\frac{dT_{av}}{dx} + R_c^2(T_c-T_{av})\frac{dR_c}{dx}$$

Using this last expression and results from the mass balances to substitute into (3), we obtain

$$\frac{dI}{dx} = (\rho_c\tilde{C}_{pc}+\rho_a\tilde{C}_{pa})\Big|_{r=R_c^-}\frac{R_c^3}{3}\frac{dT_c}{dx} + \rho_a\tilde{C}_{pa}\left[\frac{R_p^3-R_c^3}{3}\frac{dT_{av}}{dx} + R_c^2(T_c-T_{av})\frac{dR_c}{dx}\right] + \tilde{h}_c|_{r=R_c^-}M_c R_c^2\frac{a\,\rho_{SF}R_p}{3F_{SF}}(Q_{H2O}+R_1) \quad (4)$$

The continuity of the total enthalpy flux requires

$$-K\frac{\partial T}{\partial r} + \sum_i N_i h_i\Big|_{r=R_p} = \left[-K\frac{\partial T}{\partial r} + \sum N_i h_i\right]\Big|_{r=R_\delta}\left(\frac{R_\delta}{R_p}\right)^2$$

while at the outer edge of the film we have

$$\sum N_i h_i\Big|_{r=R_\delta} = N_{O_2}|_{r=R_\delta}[h_{O_2}(T_B) - h_{CO_2}(T_B)]$$

and mass balances allow us to write

$$-K\frac{\partial T}{\partial r} + \left[\sum N_i h_i\right]\Big|_{r=R_p} = -K\frac{\partial T}{\partial r}\Big|_{r=R_\delta}\left(\frac{R_\delta}{R_p}\right)^2 - Q\left(\frac{R_c}{R_p}\right)^2[h_{O_2}(T_B) - h_{CO_2}(T_B)] \quad (5)$$

If we substitute (4) and (5) into (2) and consider the following relations

$$\tilde{h}_c|_{r=R_c^-} = \tilde{h}_c(T_c) = \tilde{h}_c(T_B) + \tilde{C}_{pc}(T_c - T_B)$$

$$\Delta H_c(T_B) = h_{CO_2}(T_B) - h_{O_2}(T_B) - M_c\tilde{h}_c(T_B)$$

$$\rho_c = \rho_{SF}(1-w_{AF})(1-X)$$

$$\rho_a = \rho_{SF}w_{AF}$$

the energy balance for the solid phase finally becomes

$$F_{SF}[(1-w_{AF})(1-X)\tilde{C}_{pc} + w_{AF}\tilde{C}_{pa}]\left(\frac{R_c}{R_p}\right)^3\frac{dT_c}{dx} + F_{SF}\left[1-\left(\frac{R_c}{R_p}\right)^3\right]\tilde{C}_{pa}\frac{dT_{av}}{dx} = -K\frac{\partial T}{\partial r}\Big|_{r=R_\delta} a\left(\frac{R_\delta}{R_p}\right)^2 - \frac{d}{dx}\left(K_R\frac{dT_{PS}}{dx}\right) + a\,Q\left(\frac{R_c}{R_p}\right)^2[\Delta H_c(T_B) + M_c\tilde{C}_{pc}(T_B - T_c)] + \frac{3F_{SF}w_{AF}\tilde{C}_{pa}}{R_p^3}R_c^2(T_{av}-T_c)\frac{dR_c}{dx}$$

where by solving the energy equation for the boundary layer in terms of the unknown external solid temperature T_{PS} we find

$$-K\frac{\partial T}{\partial r}\bigg|_{r=R_\delta} = \begin{cases} \dfrac{K(T_{PS}-T_B)}{R_\delta^2\left(\dfrac{1}{R_p}-\dfrac{1}{R_\delta}\right)}; & R^* \leq R_p \\ \dfrac{K(T_{PS}-T_B)}{R_\delta^2\left(\dfrac{1}{R_p}-\dfrac{1}{R_\delta}\right)} + \dfrac{2\Delta H_w c D x_{O_2,B}}{R_\delta^2\left(\dfrac{1}{R_p}-\dfrac{1}{R_\delta}\right)} & \\ \quad - 2\Delta H_w Q_{H_2O}\left(\dfrac{R_c}{R_\delta}\right)^2; & R^* \geq R_p \end{cases} \tag{6}$$

In the ash layer, the following pseudo steady state temperature profiles are assumed to hold;

1. If the flame front is outside the particle or at the core surface

$$T = T_c + (T_{PS}-T_c)\frac{\dfrac{1}{R_c}-\dfrac{1}{r}}{\dfrac{1}{R_c}-\dfrac{1}{R_p}}; \quad R_c \leq r \leq R_p$$

2. If the flame front is in the ash layer

$$T = \begin{cases} T_c + \left[(T_{PS}-T_c) + \dfrac{2\Delta H_w Q R_c^2}{K_e}\left(\dfrac{1}{R_p}-\dfrac{1}{R^*}\right)\right]\dfrac{\dfrac{1}{R_c}-\dfrac{1}{r}}{\dfrac{1}{R_c}-\dfrac{1}{R_p}}; & \\ \qquad R_c \leq r \leq R^* & \\ T_{PS} + \left[(T_{PS}-T_c) + \dfrac{2\Delta H_w Q R_c^2}{K_e}\left(\dfrac{1}{R_c}-\dfrac{1}{R^*}\right)\right]\dfrac{\dfrac{1}{R_p}-\dfrac{1}{r}}{\dfrac{1}{R_c}-\dfrac{1}{R_p}}; & \\ \qquad R^* \leq r \leq R_p \end{cases}$$

In both cases, the assumed temperature profile is the solution of the corresponding energy equation in the ash layer with all accumulation terms neglected and obtained as a function of the solid temperature at $r = R_p(T_{PS})$ and of the core temperature (T_c) which are unknowns. With this assumed profile, the average temperature in the ash layer can be computed to render

$$T_{av} = T_c + \frac{T_{PS}-T_c}{\dfrac{1}{R_c}-\dfrac{1}{R_p}}\left[\frac{1}{R_c}+\frac{3}{2}\frac{R_c^2-R_p^3}{R_p^3-R_c^3}\right]; \qquad \begin{matrix} R^* = R_c \\ \text{or} \\ R_p < R^* < R_\delta \end{matrix}$$

$$T_{av} = \frac{3}{R_p^3-R_c^3}\left\{ T_c\frac{R^{*3}-R_c^3}{3} + \frac{T_{PS}-T_c+\dfrac{2\Delta H_w Q R_c^2}{K_e}\left(\dfrac{1}{R_p}-\dfrac{1}{R^*}\right)}{\dfrac{1}{R_c}-\dfrac{1}{R_p}}\left[\frac{R^{*3}-R_c^3}{3R_c}+\frac{R_c^2-R^{*2}}{2}\right] + T_{PS}\frac{R_p^3-R^{*3}}{3} + \frac{T_{PS}-T_c+\dfrac{2\Delta H_w Q R_c^2}{K_e}\left(\dfrac{1}{R_c}-\dfrac{1}{R^*}\right)}{\dfrac{1}{R_c}-\dfrac{1}{R_p}}\left[\frac{R_p^3-R^{*3}}{3R_p}+\frac{R^{*2}-R_p^2}{2}\right]\right\}; \quad R_c < R^* < R_p$$

If we now assume that all of the heat conducted through the ash layer which reaches the external surface of the solid phase must be released either to the gas phase by conduction through the boundary layer or by radiation to the surrounding layers of particles, we can write for an element of volume of the bed of width Δx

$$-K_e\frac{\partial T}{\partial r}\bigg|_{r=R_p^-} a\Delta x = -K\frac{\partial T}{\partial r}\bigg|_{r=R_p^+} a\Delta x - K_R\frac{dT_{PS}}{dx}\bigg|_{x+\Delta x} + K_R\frac{dT_{PS}}{dx}\bigg|_{x}$$

or

$$-K_e\frac{\partial T}{\partial r}\bigg|_{r=R_p^-} a = -K\frac{\partial T}{\partial r}\bigg|_{r=R_p^+} a - \frac{d}{dx}\left(K_R\frac{dT_{PS}}{dx}\right)$$

The assumed profile in the ash layer allows us to compute $\dfrac{\partial T}{\partial r}\bigg|_{r=R_p^-}$, while $\dfrac{\partial T}{\partial r}\bigg|_{r=R_p^+}$ can be obtained by solving the energy equation in the boundary layer. The final result for each of the three possible locations of the flame front is given in Table 1. Therefore, the energy balance in the combustion zone is split into three equations for the three different relations among the three characteristic temperatures in the solid phase: T_c, T_{PS}, and T_{av}. These equations must be solved simultaneously together with the mass balances and the energy balance for the gas phase.

A simplification can be achieved by considering the particle to be at a uniform temperature. In that case

$$T_c = T_{PS} = T_{av}$$

and the energy balance reduces to a single equation

$$F_{SF}\left[(1-X)(1-w_{AF})\tilde{C}_{pc}\left(\frac{R_c}{R_p}\right)^3 + w_{AF}\tilde{C}_{pa}\right]\frac{dT_c}{dx} = -a\left(\frac{R_\delta}{R_p}\right)^2 K\frac{\partial T}{\partial R}\bigg|_{r=R} - \frac{d}{dx}\left(K_R\frac{dT_{PS}}{dx}\right) + aQ\left(\frac{R_c}{R_p}\right)^2[\Delta H_c(T_B) + M_c\tilde{C}_{pc}(T_B-T_c)]$$

where $K\dfrac{\partial T}{\partial r}\bigg|_{r=R}$ is still given by Equation (6) but now with $T_{PS} = T_c$. While undoubtedly there is a temperature drop in the ash layer, it develops only in the later stages of the combustion reaction, as the numerical results for the extended model show, and hence most of the heat has already been released. Whether it is necessary to consider the more complicated case can only be determined by comparing the two cases numerically.

An energy balance for the bulk gas phase can be written for a differential element of volume of the bed as

$$\sum_i \frac{d}{dx}(Gg_ih_i) = \sum_i N_ih_i\bigg|_{r=R_\delta} a\left(\frac{R_\delta}{R_p}\right)^2$$

TABLE 1. EQUATION FOR T_{PS} ASSUMING FLUX CONTINUITY AT $r = R_p$

Case 1: Flame front at core

$$\frac{K_e(T_c - T_{PS})}{R_p^2\left(\frac{1}{R_c} - \frac{1}{R_p}\right)} = \frac{K(T_{PS} - T_B)}{R_P^2\left(\frac{1}{R_p} - \frac{1}{R_\delta}\right)} - \frac{1}{a}\frac{d}{dx}\left(K_R\frac{dT_{PS}}{dx}\right)$$

Case 2: Flame front in boundary layer

$$\frac{K_e(T_c - T_{PS})}{R_p^2\left(\frac{1}{R_c} - \frac{1}{R_p}\right)} = \frac{K(T_{PS} - T_B)}{R_p^2\left(\frac{1}{R_p} - \frac{1}{R_\delta}\right)} + \frac{cDx_{O_2,B}2\Delta H_w}{R_p^2\left(\frac{1}{R_p} - \frac{1}{R_\delta}\right)} - \frac{1}{a}\frac{d}{dx}\left(K_R\frac{dT_{PS}}{dx}\right)$$

Case 3: Flame front in ash layer

$$\frac{T_c - T_{PS} + \frac{2\Delta H_w Q R_c^2}{K_e}\left(\frac{1}{R^\circ} - \frac{1}{R_c}\right)}{\frac{1}{K_e}\left(\frac{1}{R_c} - \frac{1}{R_p}\right)R_p^2} = \frac{K(T_{PS} - T_B)}{R_p^2\left(\frac{1}{R_p} - \frac{1}{R_\delta}\right)} - \frac{1}{a}\frac{d}{dx}\left(K_R\frac{dT_{PS}}{dx}\right)$$

$$-K\frac{\partial T}{\partial r}\bigg|_{r=R_\delta} a\left(\frac{R_\delta}{R_p}\right)^2$$

Performing the indicated differentiation and introducing results from the mass balances, we get

$$\sum_i Gg_i\frac{dh_i}{dx} = -K\frac{\partial T}{\partial r}\bigg|_{r=R_\delta} a\left(\frac{R_\delta}{R_p}\right)^2$$

Since

$$\frac{dh_i}{dx} = C_{pi}\frac{dT_B}{dx}$$

if we define an average heat capacity for the mixture by

$$<C_p> = \sum g_i C_{pi}$$

the temperature equation for the gas phase turns out to be

$$G<C_p>\frac{dT_B}{dx} = -K\frac{\partial T}{\partial r}\bigg|_{r=R_\delta} a\left(\frac{R_\delta}{R_p}\right)^2$$

where again $K\frac{\partial T}{\partial r}\Big|_{r=R_\delta}$ is given by Equation (6).

DEVELOPMENT OF EQUATIONS FOR GASIFICATION ZONE

The set of reactions to be considered is

$$R3: \quad C + H_2O \rightarrow CO + H_2 \quad ; \quad Q_{H_2O}$$

$$R4: \quad CO + H_2O \rightarrow CO_2 + H_2$$

$$R5: \quad C + 2H_2 \rightarrow CH_4 \quad ; \quad R_5$$

The gasification by carbon dioxide is omitted from the set because its effect is introduced through the water gas shift reaction. The I.G.T. research showed that there were no diffusional or mass transfer limitations over a wide range of parameters, and so concentrations within the particle will be considered to be the same as in the bulk phase. The pseudo steady state assumption is used in the derivation of the mass balances. Mass balances are written for those species or pseudo species whose concentrations are not changed by the water gas shift reaction which is considered to be in equilibrium. Thus

$$N_{H_2O} + N_{CO_2} = -Q_{H_2O}$$

$$N_{CH_4} = R_5$$

$$K_{ws} = \frac{g_{CO_2}\cdot g_{H_2}}{g_{CO}\cdot g_{H_2O}}$$

Performing a shell balance for the i^{th} species in a differential element of volume in the reactor, we can write

$$-\frac{d(Gg_i)}{dx} + a\,N_i = 0$$

A total mass balance for the gas phase gives

$$\frac{dG}{dx} = M_c\,a(Q_{H_2O} + R_5)$$

If we call

$$\xi = g_{H_2O} + g_{CO_2}$$

then the rate of change for ξ and g_{CH_4} can be written as

$$G\frac{d\xi}{dx} = -a[(1 + M_c\xi)Q_{H_2O} + M_c\xi R_5]$$

$$G\frac{dg_{CH_4}}{dx} = a[-M_c\,g_{CH_4}Q_{H_2O} + (1 - M_c g_{CH_4})R_5]$$

The mass flow rate of the gas phase and the concentrations of the dependent species can be written now in terms of the values of g_{H_2O}, g_{CO_2}, and g_{CH_4} and the conditions at the transition between zones (indicated by subscript 1); their expressions are

$$G = \frac{G_1[1 + M_c(\xi_1 - g_{CH_4,1})]}{1 + M_c(\xi - g_{CH_4})}$$

$$g_{CO} = \frac{1 + M_c(\xi - g_{CH_4})}{1 + M_c(\xi_1 - g_{CH_4,1})}(g_{H_2O,1} + 2g_{CO_2,1} + g_{CO,1}) - g_{H_2O} - 2g_{CO_2}$$

$$g_{H_2} = \frac{1 + M_c(\xi - g_{CH_4})}{1 + M_c(\xi_1 - g_{CH_4,1})}(g_{H_2O,1} + g_{H_2,1} + 2g_{CH_4,1}) - g_{H_2O} - 2g_{CH_4}$$

At the transition between zones

$$g_{H_2,1} = g_{CO,1} = g_{CH_4,1} = 0$$

$$g_{O_2,1} = 0$$

$$G_1 = G^o(1 + M_c g^o{}_{O_2})$$

$$g_{H_2O,1} = \frac{g^o{}_{H_2O}}{1 + M_c g^o{}_{O_2}}$$

$$g_{N_2,1} = \frac{g^o{}_{N_2}}{1 + M_c g^o{}_{O_2}}$$

$$g_{CO_2,1} = \frac{g^o{}_{O_2} + g^o{}_{CO_2}}{1 + M_c g^o{}_{O_2}}$$

and consequently

$$\xi_1 = g_{CO_2,1} + g_{H_2O,1} = \frac{g^o{}_{CO_2} + g^o{}_{O_2} + g^o{}_{H_2O}}{1 + M_c g^o{}_{O_2}}$$

The change of core conversion along the gasification zone is found to be

$$\frac{dX}{dx} = -\frac{M_c\, a(Q_{H_2O} + R_5)}{F_{SF}(1 - w_{AF})}$$

An energy balance similar to the one obtained for the combustion zone with the additional assumption of uniform particle temperature can be written. The final expression obtained once the mass balance results are introduced is

$$F_{SF}[1 - X(1 - w_{AF})]C_s \frac{dT_p}{dx} = -\frac{d}{dx}\left(K_R \frac{dT_p}{dx}\right) + \frac{aK(T_p - T_B)}{R_p^2\left(\frac{1}{R_p} - \frac{1}{R_\delta}\right)} + a[Q_{H_2O}\Delta H_3 + R_5\Delta H_5] + \Delta H_4 \frac{d}{dx}(Gg_{CO_2})$$

By an analysis similar to that for the combustion zone, the temperature equation for the gas phase can be written:

$$G\langle C_p\rangle \frac{dT_B}{dx} = \frac{aK(T_p - T_B)}{R_p^2\left(\frac{1}{R_p} - \frac{1}{R_\delta}\right)}$$

BOUNDARY CONDITIONS

The reactor has been described by a complex system of algebraic and ordinary differential equations. For the ordinary differential equations, conditions are specified at both ends of the reactor and at an intermediate point, the transition between zones, the position of which is not known a priori and must be obtained during the course of the solution of the problem. Therefore, we can visualize our model as a multipoint boundary-value problem. The combustion zone is described by a seventh-order and the gasification zone by a sixth-order system of ordinary differential equations, and thirteen boundary conditions must be specified. In fact, fourteen conditions can be established, the additional one providing us with information which enables us to compute the position of the transition between zones in much the same way that the location of the flame front is obtained in the single-particle studies. At the top of the gasifier we can specify the conversion of the solid feed ($X = 0$, $x = L$) and the temperature of the solid in the feed ($T_p = T_{p2}$, $x = L$). At the transition between zones (x^*) we can specify that no ash layer has been formed in the particles entering the combustion zone, so $R_c = R_p$, $X = x^*$, and no oxygen leaves the combustion zone, $g_{O_2} = 0$, $x = x^*$. Also, no methane leaves the combustion zone, $g_{CH_4} = 0$, $x = x^*$. The amount of water and carbon dioxide leaving the combustion zone is known ($\xi = \xi_1$, $x = x^*$), and as no ash layer has been formed before entering the combustion zone, the core and surface temperatures are the same ($T_c = T_{PS}$, $x = x^*$). We must have temperature continuity of the solid phase ($T_p|_{x_+^*} = T_c|_{x_-^*}$, $x = x^*$) as well as gas temperature continuity ($T_B|_{x_+^*} = T_B|_{x_-^*}$). Also, the solid conversion must be continuous ($X|_{x_+^*} = X|_{x_-^*}$, $x = x^*$), and the flux of radiation must satisfy

$$-K_R \frac{dT_P}{dx}\bigg|_{x_+^*} = -K_R \frac{dT_{PS}}{dx}\bigg|_{x_-^*}; \quad x = x^*$$

At the bottom of the gasifier we can specify that the temperature of the gaseous stream entering the gasifier is known ($T_B = T_B^o$, $x = 0$) as well as the concentration of oxygen in the feed ($g_{O_2} = g^o_{O_2}$, $x = 0$). The radiation losses there are

$$K_R \frac{dT_{PS}}{dx} = h(T_{PS}^4 - T_W^4); \quad x = 0$$

Since T_W is an unknown, assumptions must be made as to its value. Two natural possibilities arise: either the bottom is well insulated and therefore $T_W = T_{PS}$, or it is at the temperature of the entering gaseous stream $T_W = T_B^o$. Under the usual operating conditions, the solid leaves the gasifier at almost the same temperature as the gaseous stream enters, as our computations show (development of a large ash layer at the bottom of the reactor), and both assumptions coincide.

NUMERICAL SOLUTION

Marching methods were disastrously unsuccessful. Even simplified versions of the problem that reduced the number of unknowns to be estimated at either end of the reactor did not render any results. The intrinsic stiffness of the system of ordinary differential equations indicates that implicit methods (finite-difference approximation) should be employed, and this was the approach used. Satisfactory results were obtained, although slow convergence resulted from the large damping factor that was required to avoid oscillations. The solution should provide not only the profiles along the reactor but also the relative size of each of the two zones. This fact precluded the use of a complete quasilinearization scheme, although linearization with respect to some of the variables was used, at least with respect to those where the most severe nonlinearities appear (mainly particle temperature or core temperature in the case of the combustion zone). A description of the method can be supplied to the reader.

Initial studies were made neglecting any temperature gradient in the ash layer. Furthermore, it was assumed that no methane was formed anywhere in the gasifier. This rather simplified model, however, shows the essential features of the reactor behavior, and an independent discussion of its numerical results is warranted. A gaseous feed mass flow rate of 0.098 g cm^{-2} s^{-1} was assumed. The inlet composition was 12% oxygen and 88% steam (by volume) at an operating pressure of 20 atm. The solid feed was considered to be devolatilized char with 27% by weight of ash and 73% carbon. The solid particles were taken to be spheres 2 cm in diameter, with a reactivity factor (for the Johnson kinetic model) $f_o = 1$. The gas phase entered at 600°K, while the solid inlet temperature was assumed to be 300°K. One of the objectives was to study the effect of changing the solid feed mass flow rate F_{SF}. For F_{SF} values larger than 0.0278 g cm^{-2} s^{-1}, oxygen was completely consumed at the bottom of the gasifier in a thin zone about 5 cm thick, and the gasification zone practically occupies the whole reactor. The carbon in the char is not completely spent, and an unreacted residue leaves the gasifier together with the ash. If the solid feed mass flow rate is reduced below the aforementioned value, practically all of the carbon reacts and an ash layer, whose thickness is highly sensitive to changes in F_{SF}, begins to develop. In Figure 1 the temperature profile for the solid phase has been plotted for different solid feed rates within the range of 0.025 to 0.030 g cm^{-2} s^{-1}. In obtaining such graphs, radiation effects were neglected. They will later be incorporated into the model. Labels A and B in each curve indicate the points where the oxygen consumption initiates and terminates, respectively. Oxygen in all the cases has reacted completely in a layer about 5 cm thick, but such a layer can be located either at the bottom or in the middle of

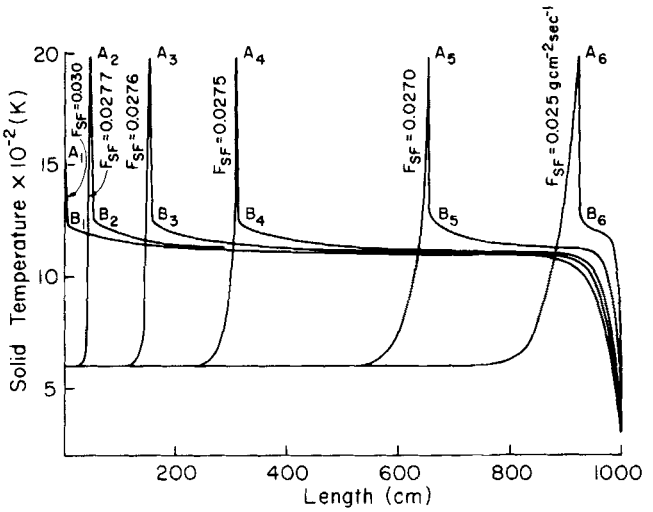

Fig. 1. Effect of changes in solid feed mass flow rate on the solid temperature profile. Methanation reaction neglected. No radiation. Particle at uniform temperature.

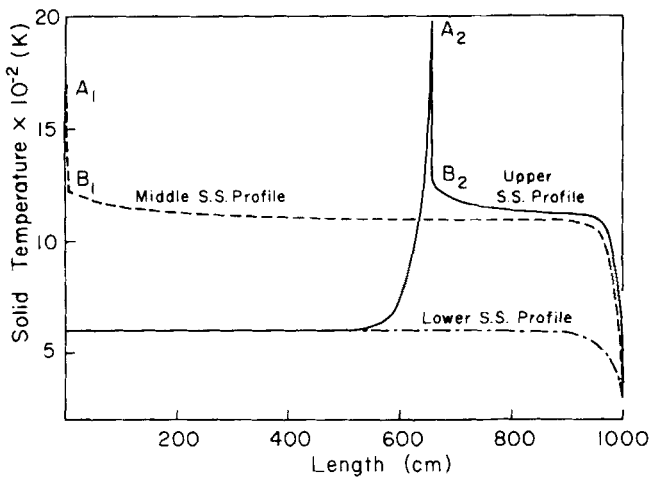

Fig. 3. Multiple steady state solid temperature profiles.

the gasifier, depending on the values of F_{SF}.

The maximum temperature attained in the solid phase is almost independent of the value of F_{SF} provided it is low enough for an ash layer to develop within the reactor ($T_{c,\max} = 1\,980°K$). If such a condition is not met, $T_{c,\max}$ is always located at the very bottom of the gasifier and decreases with increasing values of the solid feed rates, as is shown in Figure 6. The great sensitivity of the ash-layer thickness to changes in values for F_{SF} is shown in Figure 1. There we can see that a change from $F_{SF} = 0.0275$ g cm^{-2} s^{-1}, which is less than a 1% decrease, increases the ash-layer thickness from 46 to 309 cm, and hence the small inevitable variations in the solid flow rate in actual operation will leave the position of the hot spot in doubt. In Figure 2 ash-layer thickness vs. F_{SF} has been plotted. The steepness of the curve for values of F_{SF} larger than 0.027 g cm^{-2} s^{-1} is another indication of the already mentioned sensitivity. The thin zone of oxygen consumption travels two-thirds of the reactor length in the narrow range $0.027 \leq F_{SF} \leq 0.02774$.

Steady State Multiplicity

While we attempted to solve the problem for a mass flow rate of the solid feed of 0.027 g cm^{-2} s^{-1}, no convergence was obtained. Furthermore, in the iterative scheme used, while the results of one iteration indicated the existence of a thick ash layer, the next one showed that no such ash layer was present. This numerical behavior suggested the existence of two different solutions of the boundary-value problem for the given set of parameters. To investigate that possibility and separate the solutions, the following scheme was developed.

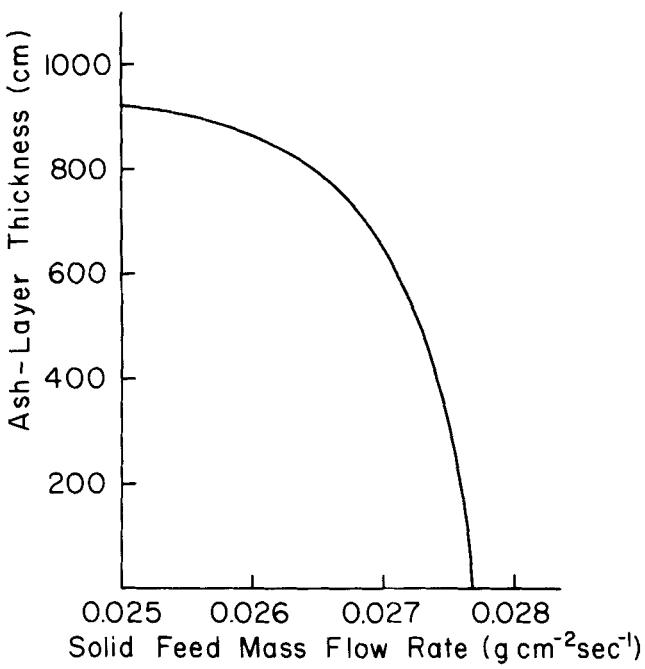

Fig. 2. Ash-layer thickness as a function of solid feed mass flow rate. Methanation reaction neglected. No radiation. Particle at uniform temperature.

1. Solve the problem for $F_{SF} = 0.030$ g cm^{-2} s^{-1} for which it was already known from previous numerical computations that no ash layer was formed.

2. Use the profiles so obtained as initial guesses for a new reactor for which $F_{SF} = F_{SF}$ (previous) $- 0.0005$ and repeat the procedure until a reactor for which $F_{SF} = 0.027$ g cm^{-2} s^{-1} was solved.

3. Starting from a reactor with a solid feed rate of 0.025 g cm^{-2} s^{-1} for which an ash layer 925 cm deep was known to develop, the same procedure was used, but now increase F_{SF} by 0.0005 g cm^{-2} s^{-1} each time.

As a result of such computations, two different profiles were obtained, one with an ash layer of about 650 cm and the other with no ash layer. A program was developed to investigate whether for these feed conditions the unignited steady state, that is, one for which all of the oxygen is not consumed within the reactor, could still occur. A simple finite-difference scheme was established. Very fast convergence was obtained for a reactor where negligible reaction occurs, that is, with a reactor acting as a countercurrent heat exchanger. In Figure 3 the solid temperature profiles for these three steady states are shown. In Figure 4 several properties of the system are given as functions of the solid feed rate for each of the two upper branches (the unignited steady state is omitted because of its irrelevancy) in which the solution is split. No attempt was made to connect both branches through an unstable intermediate steady state if such be the case. It is shown there that for $F_{SF} = 0.027$ g cm^{-2} s^{-1}, the difference in final conversion between the steady states is not complete vs. $X_f = 0.967$, and the difference in temperature of the gaseous stream leaving the gasifier is 979°K vs. 1 012°K. This holds true for the whole multiplicity region for which $0.0265 < F_{SF} < 0.02774$.

Observe in Figure 4 the rapid increase in the temperature of the gases leaving the gasifier when the solid feed rate is decreased below the lower bound of the multiplicity region. The energy supply to the gasifier (through the

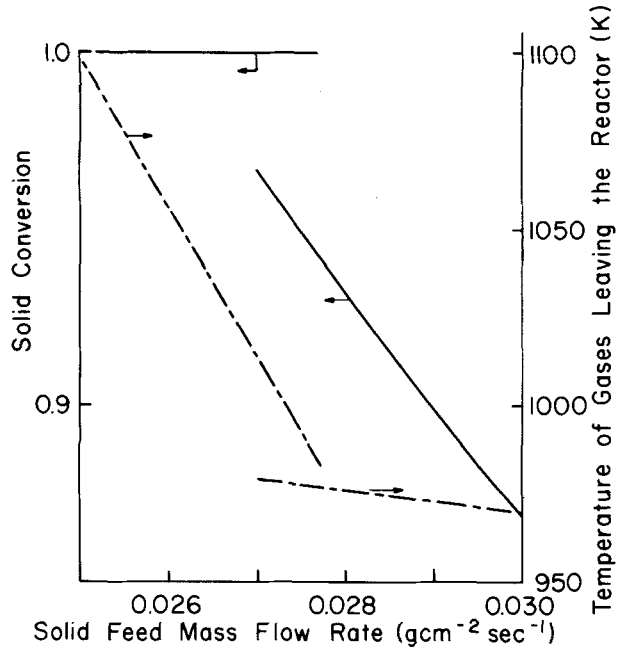

Fig. 4. Difference in properties between steady state profiles. Multiplicity region.

oxygen input and sensible heat in the steam) is in excess of the amount needed to gasify the coal fed to it. For coal feed rates larger than the upper bound, coal leaves partially reacted and also at its maximum temperature. Therefore, we can expect that the optimum operating conditions will fall within the multiplicity region, which at the same time coincides (see Figure 2) with the region of highest sensitivity of the traveling oxygen consumption zone: $0.027 \leq F_{SF} \leq 0.02774$. This behavior strongly suggests operating difficulties in practice. The maximum temperature achieved in the solid phase is excessively high for complete conversion conditions as shown in Figure 6, greatly exceeding the ash fusion point. Since radiation effects were neglected, no final word can be said about the

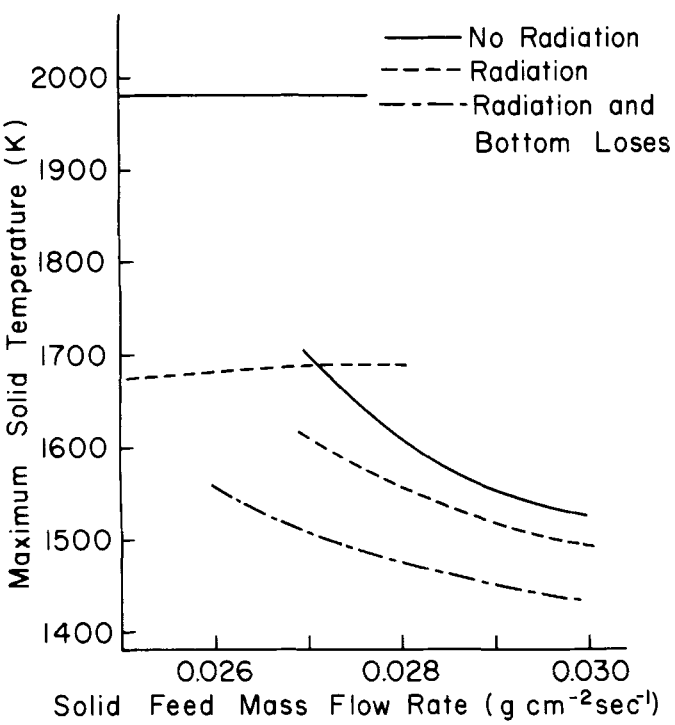

Fig. 6. Effect of the radiation and of radiant heat losses from reactor bottom on the maximum solid temperature.

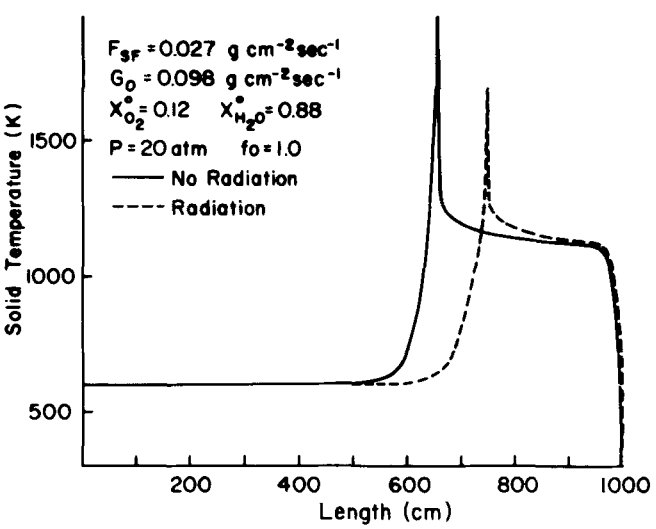

Fig. 5. Comparison between steady state profiles with and without considering radiation for the case of a deep ash-layer formation.

maximum solid temperature until it is included in the model.

Effect of Radiation

In considering radiation within the reactor, the emissivity of a coal particle can be considered to be between 0.75 and 0.9, and in most of this study a conservative value of 0.75 was adopted. Effects of variations in the values of this parameter within the whole range 0 to 1 are discussed later when the most complete reactor model studied is under consideration. If oxygen is consumed at the very bottom of the gasifier, the main difference introduced by radiation is the lowering of the maximum solid temperature. For $F_{SF} = 0.027$ g cm^{-2} s^{-1} and no ash-layer formation (lower branch), the predicted value of 1 700°K obtained under the assumption of negligible radiation is reduced to about 1 611°K. If, in addition, it is assumed that the inner walls at the bottom of the reactor are at the inlet gas temperature rather than at the outlet solid temperature (implying that heat losses through the bottom occur), this maximum is further lowered to a value about 1 515°K. The solid conversion is reduced from 96.7 to 95.9% if radiation is included. If, in addition, heat losses through bottom are considered, a lower value of 93.1% is predicted. In Figure 5 results are shown for the same value of F_{SF} (0.027 g cm^{-2} s^{-1}) but with a deep ash layer developed in the bed (upper branch). Under these conditions the gas inlet and the solid outlet temperature are the same, so no distinction is made about the inner wall temperature at the bottom of the reactor. In that figure it can be seen that there is a dramatic lowering of the peak temperature from 1 980° to 1 690°K, approximately. Again, as it was in the case of no radiation, the maximum solid temperature is practically the same for all solid feed rates provided an ash layer is present. Otherwise it decreases with increasing values of F_{SF} as can be seen in Figure 6.

In Figure 6 the maximum solid temperature has been plotted against the solid feed rate. Results for negligible radiation were also included. The existence of two branches of solutions is shown. The lower branch with radiation included is split into two different cases: with and without radiant heat losses from the bottom of the bed. The upper branch for these two cases is the same, as we have already pointed out. In that figure it can be seen that the size of the multiplicity region is enhanced when radiation is taken into account. The more efficient use of the heat released in the combustion zone implies that a larger amount of

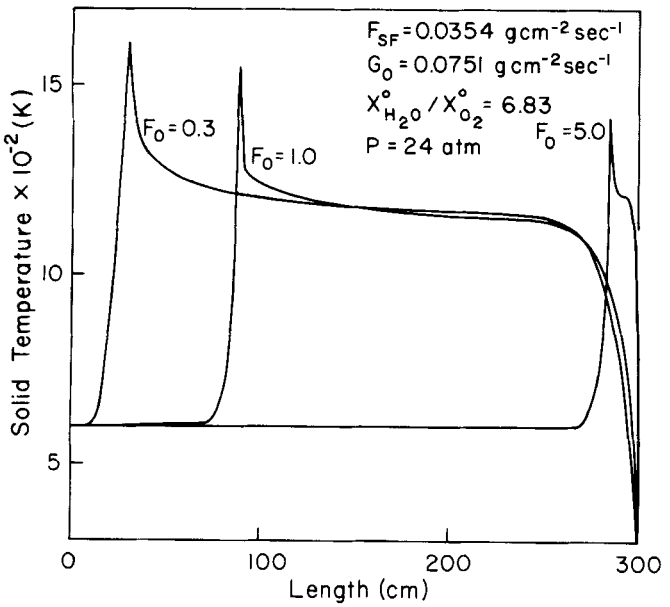

Fig. 7. Solid temperature profiles for different coal reactivities. Methanation reaction and radiation effects included. Particle at uniform temperature.

solid can be completely gasified within the reactor. Consequently, the upper branch extends further to the right. On the other hand, when radiation losses from the bottom of the bed are considered, it is possible to lose enough heat so even smaller solid feed rates can pass through the gasifier without complete conversion. For example, at $F_{SF} = 0.026$ g cm^{-2} s^{-1}, for which it was predicted that there would be complete conversion if radiation was neglected, or if included but without bottom losses, there will be two solutions: complete and 96.3% conversion.

The Methanation Reaction

The formation of methane is an additional exothermic mechanism of carbon consumption. By including it, a larger coal throughput can be expected to be completely gasified in the reactor for a given oxygen input. This is due to the exothermicity of the methanation reaction which by releasing heat in the same location where the endothermic steam gasification is taking place decreases the energy input requirements. This qualitative reasoning was proved to be true numerically. Loads with a ratio of 3.47 moles of carbon per mole of oxygen were completely gasified vs. a maximum of 2.87 achieved when the methane formation was neglected. The predicted value of the maximum tem-

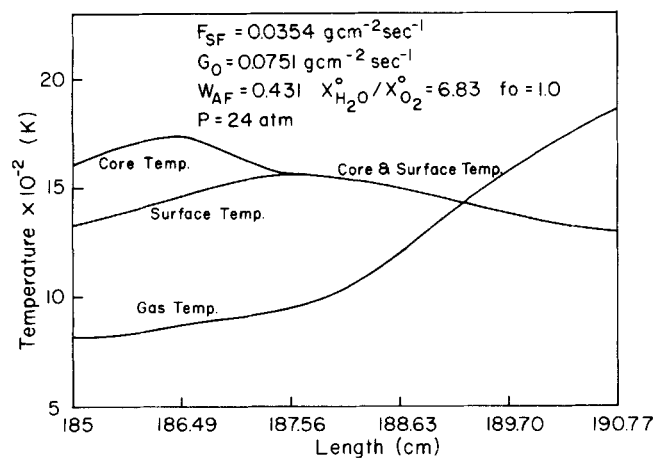

Fig. 9. Gas-phase, core, and solid external surface temperature profiles in the zone of rapid oxygen consumption when allowances are made for temperature gradients in the particle ash layer.

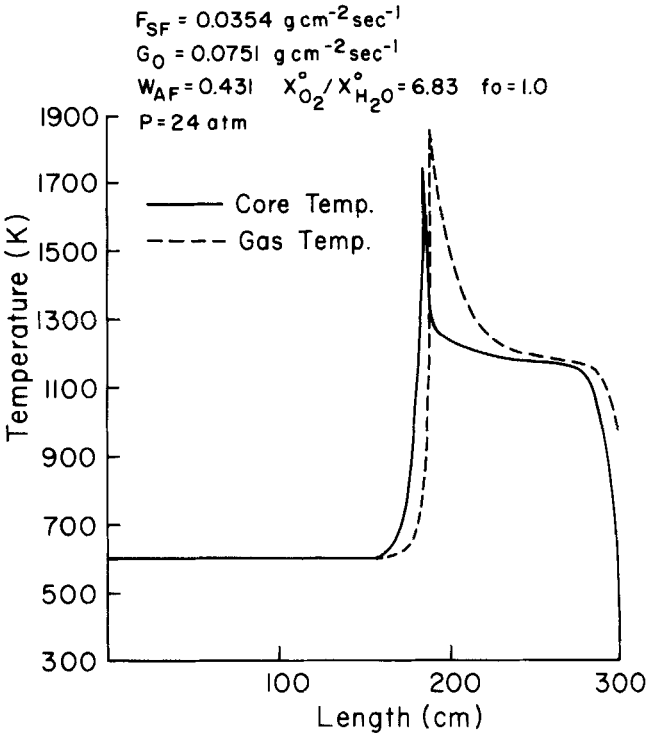

Fig. 8. Gas phase and core temperature profiles when allowances are made for temperature gradients in the particle ash layer.

perature of the solid phase was reduced from 1 690°K to 1 545°K, even though the steam-oxygen ratio in the gaseous feed was decreased from 7.33 to 6.83, and it is known experimentally that the lower the ratio the greater the maximum temperature. The length of the bed was reduced from 10 to 3 m when the operating pressure was increased from 20 to 24 atm also. In Figure 7 the temperature profile obtained for the solid phase is plotted for three different reactivity factors. The main operating conditions are indicated in the graph. Observe the increase of the ash-layer depth and the lowering of the solid maximum temperature as the reactivity factor increases (1 610°K, 1 545°K, and 1 415°K are the predicted values for reactivity factors 0.3, 1.0, and 5.0, respectively). Although no plot is presented to avoid unnecessary repetitions, it should be pointed out that the same type of steady state multiplicity and ash-layer depth sensitivity was found, as was the case when the methanation reaction was neglected.

Particle Ash-Layer Temperature Gradients

A more realistic model should consider the existence of temperature gradients within the particle ash layer if a progressive shell model is assumed for a typical particle within the reactor combustion zone. In such a model the temperature at three different places (but at the same reactor cross section) are of interest: in the gas phase, in the core, and at the external surface of the particle. In Figure 8, for the set of conditions indicated on the graph, the core and gas phase temperature profiles are shown. As the particle does not start shrinking until it is well within the combustion zone, the profiles of core and external surface temperatures coincide all along the gasification zone.

In Figure 9 the three temperature profiles are shown (for the same set of conditions as in Figure 8) for the zone of rapid oxygen consumption. We can see the start of core formation indicated by the separation of the core and external surface temperature profiles. The three temperatures approach each other very rapidly in the deep ash layer that is formed at the bottom of the reactor in such a way that the particle leaves the gasifier at a temperature that is practically uniform throughout and equal to the

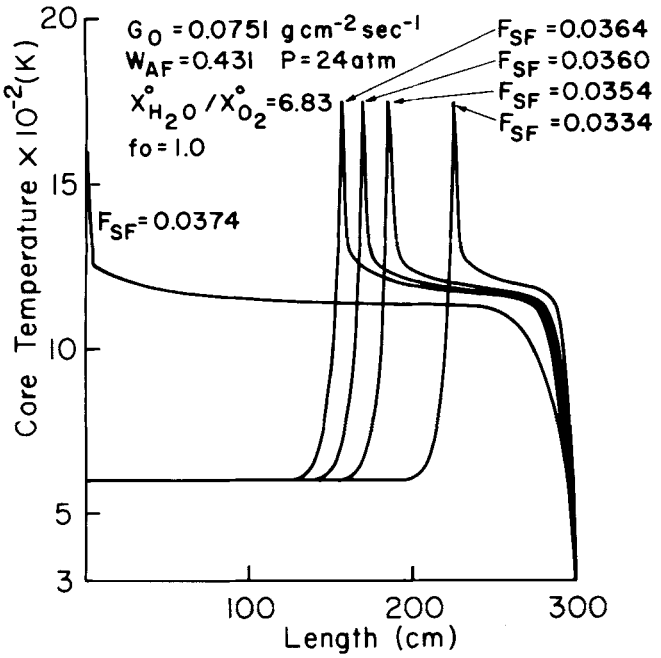

Fig. 10. Effect of changes in solid feed mass flow rate on the core temperature profiles. Methanation reaction and radiation effects included. Temperature gradients in ash layer considered.

inlet gas temperature. Combustion occurs mainly in the boundary layer (core shrinkage does not start until the solid conversion has exceeded 96.5%), explaining why the gas phase can reach a higher temperature than the particle.

In all the runs made with incomplete carbon consumption, the flame was always in the boundary layer, and no core shrinkage occurred. The final conversion achieved in those cases was lower than 96.5%.

Ash Layer Depth Sensitivity Studies

To explore the already mentioned sensitivity of the ash-layer thickness to slight variations in the carbon/oxygen ratio, a gaseous feed of 0.0751 g cm^{-2} s^{-1} with a steam/oxygen ratio of 6.83 was assumed. An operating pressure of 24 atm and a coal with a reactivity factor f_o equal to 1.0 was considered. The ash mass fraction was taken to be 0.431. The solid feed rate was changed from 0.0314 to 0.0374 g cm^{-2} s^{-1}, and consequently the C/O ratio range explored extended from 3.07 to 3.67 moles of fixed carbon per mole of oxygen. Figure 10 shows the resulting core temperature profiles. Thus, if an ash layer is formed, the curves show a maximum practically independent of changes in the C/O relation and equal to 1 745°K. The same is true for both the gas phase and solid external surface temperatures, 1 855° and 1 555°K, respectively.

It can also be observed that for C/O ratios below 3.56 ($F_{SF} = 0.0364$), an ash layer larger than half the bed height is developed, while if it is increased to 3.66 ($F_{SF} = 0.0374$), no such ash layer occurs. Neither is all of the carbon consumed ($X_f = 0.962$). The possibility of multiple steady states was not investigated in this case.

Figure 11 shows how changes in the C/O ratio affect the amount of gaseous species produced per gram of carbon fed (products of the devolatilization process are not taken into account). There it can be seen that while the methane production steadily increases, the total production of hydrogen and carbon monoxide presents a definite maximum for a value of C/O ratio of about 3.35. Consequently, the heat content of the gaseous products, that is, the heat they would release if burnt, shows a maximum at about 3.6 for the C/O ratio, as is also shown in Figure 11. Since the steam feed rate is fixed for all these

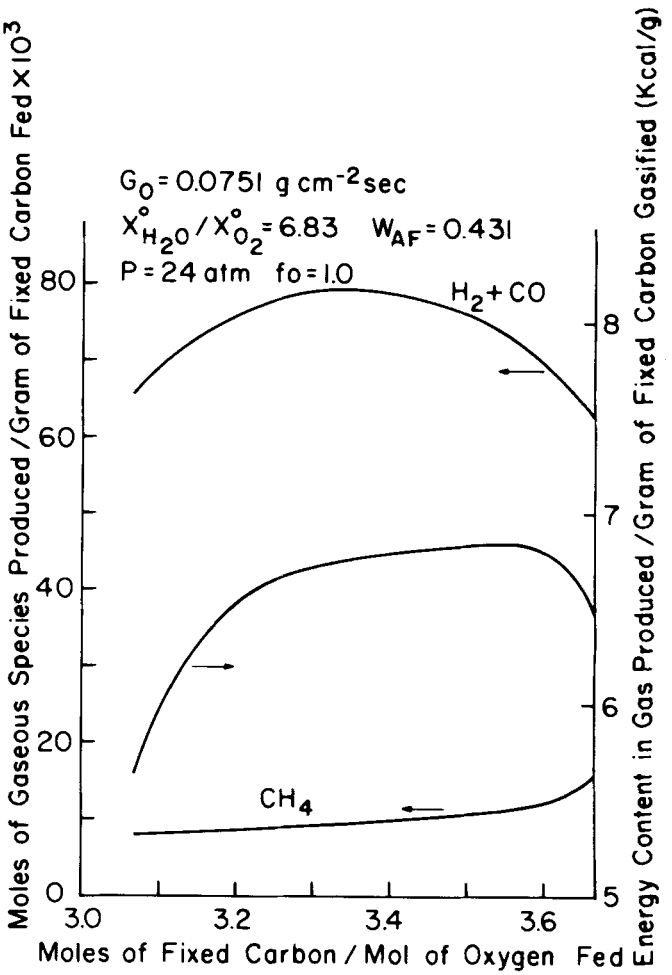

Fig. 11. Effect of changes of the C/O molar ratio in feed on the moles of gaseous species produced per unit mass of fixed carbon fed to the gasifier and on the energy content of the gaseous product.

calculations, such a plot indicates the optimum operation from a thermal efficiency point of view. It should be pointed out that these optimum conditions coincide with the region of maximum sensitivity, and therefore problems regarding operational controllability might be expected. In Figures 12 and 13 the predicted concentration profiles of the gaseous species are shown for two typical cases of complete and incomplete carbon conversion. Observe that the carbon monoxide profile shows a maximum which occurs about the point where the coal particle begins to be gasified, that is, near the upper end of the

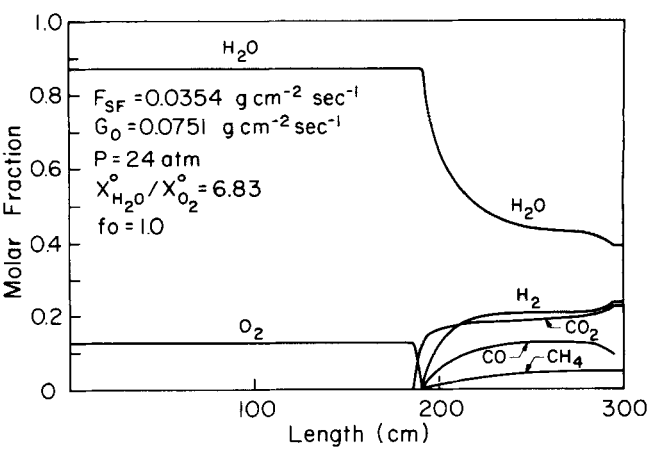

Fig. 12. Concentration profiles for a typical case of complete carbon conversion in the reactor.

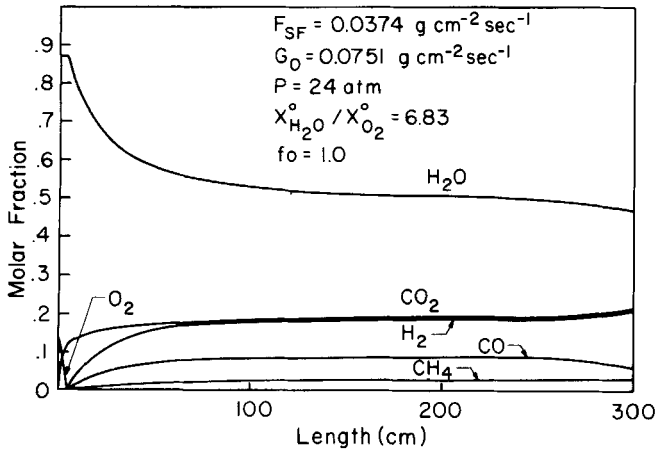

Fig. 13. Concentration profiles for a typical case of incomplete carbon conversion in the reactor.

reactor where the solid temperature is low enough to stop the gasification reactions. However, the equilibrium assumption, made on the water gas shift reaction, implies that this reaction is still occurring and all the changes in composition from this point up are due to shift in the equilibrium constant (which increases for lower temperature values). In our case, we have assumed the water gas shift reaction to be frozen at 1 000°K. (This is the reason why the profiles of all the species involved in this reaction end in a straight line as shown in Figure 12.) However, it may also happen that such an equilibrium freezing occurs at a higher temperature, roughly that which occurs at the point of maximum concentration of carbon monoxide, as we shall discuss when the effect of changing the steam/oxygen ratio in the feed is studied. Because of this uncertainty, the total amount of both hydrogen and carbon monoxide produced was plotted instead of the corresponding values for each of the two species.

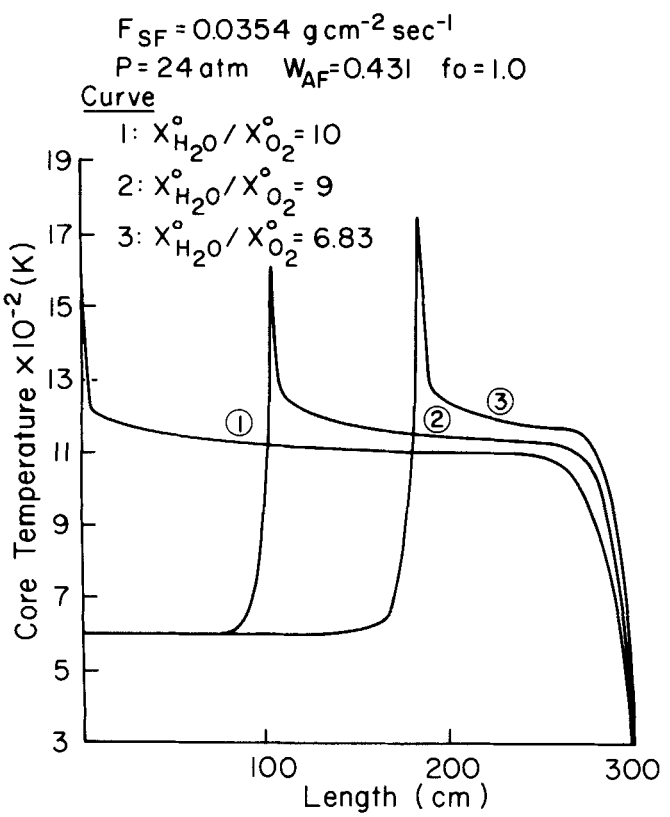

Fig. 15. Effect of changes in the steam-oxygen feed ratio on core temperature profiles.

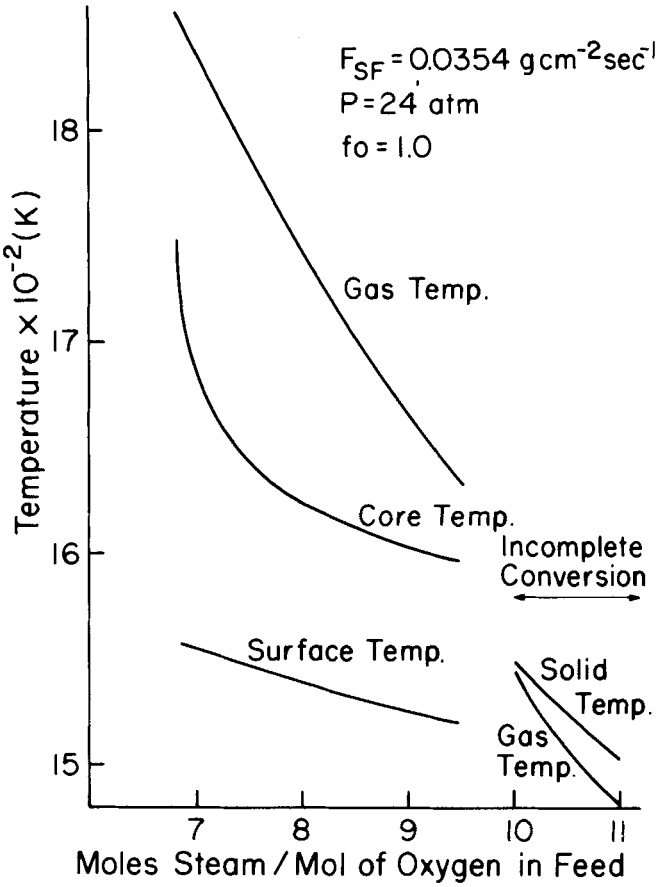

Fig. 14. Effect of changes in the steam-oxygen feed ratio on maximum temperatures.

Because of the small exothermicity of the reaction, besides the prediction of the hydrogen/carbon monoxide yield ratio, which is not a significant parameter of operation, no major effect of this uncertainty should be expected. Furthermore, the difference, if any, will affect the upper region of the reactor where the unaccounted for devolatilization process is also occurring.

Effects of Changing the Steam/Oxygen Ratio in Gas Feed

This is one of the major operating variables in the control of the bed. By changing the steam/oxygen ratio the maximum temperature obtained in the reactor can be set below the ash melting point. To study this operational parameter, a coal with a reactivity factor f_o equal to 1.0 at a feed rate of 0.0354 g cm^{-2} s^{-1} and an ash mass fraction of 0.431 was assumed. The carbon/oxygen relation was kept equal to 3.47. The steam/oxygen ratio was changed by adding more steam to the inlet gaseous stream, and the range studied was from 6.83 to 11. The maximum gas phase, core, and external solid surface temperature achieved are shown in Figure 14. Figure 15, on the other hand, shows the core temperature profiles obtained for some of the runs. (The corresponding steam/oxygen ratios are shown on the graphs.) In Figure 14 both core and gas phase temperature are affected greatly by changes in the steam oxygen feed ratio. By increasing them, the maximum temperature decreases very rapidly until the point where complete carbon conversion is no longer possible. This transition occurs between the values 9.5 and 10.0 for the steam/oxygen ratio. Accompanying the transition, the region of rapid oxygen consumption moves greatly, as shown in the temperature profiles in Figure 15. The water/oxygen ratio also affects the outlet hydrogen/carbon monoxide ratio, which also depends on the type of coal gasified as pointed out by Rudolph (1974). The predicted hydrogen/carbon monoxide ratio both at the reactor outlet

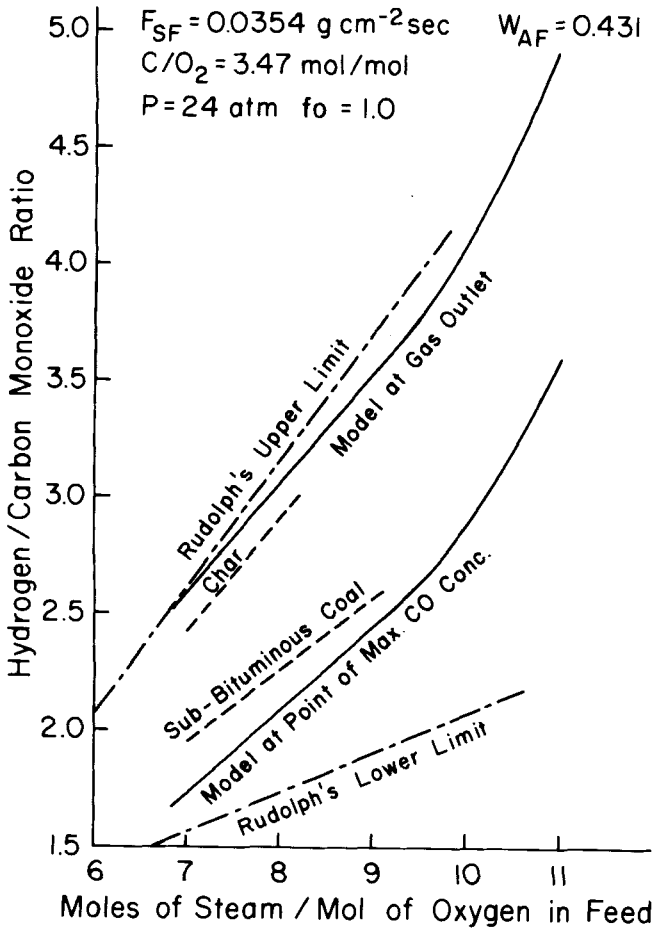

Fig. 16. Hydrogen/carbon monoxide ratio vs. water/oxygen ratio in feed. Comparison of model predictions with Rudolph's experimental results.

as well as the point within the bed where the carbon monoxide concentration reaches its maximum is plotted in Figure 16. We can see that both curves fall within the upper and lower experimental limits given in Rudolph's paper for different types of coals (curves for two of them, char and subbituminous coal are also presented). The qualitative agreement between the predicted and experimental effect is satisfactory, but no quantitative prediction can be made. This is of no critical significance because the heat content of both hydrogen and carbon monoxide is practically the same, and, as Rudolph points out, for high British thermal unit gas production, the hydrogen/carbon monoxide ratio is adjusted in a later stage of the whole process before the methanation step.

Effect of Changes in Pressure

The most economical operating pressure must be determined for the process in its entirety, including later stages to be carried out after gasification. We will limit ourselves here to the effect of changes in pressure on the gasification stage only. Increases in pressure allow larger amounts of carbon to be completely gasified as is shown in Figure 17, where the core temperature profile for the feed conditions indicated but at two different levels of operating pressures are shown. If P is reduced from 24 to 12 atm, an incomplete carbon conversion is obtained. Moreover, larger amounts of methane per unit mass of fixed carbon gasified are produced at higher pressures, as shown in Figure 18. There it can be seen that this effect shows a leveling off in the range of 25 to 30 atm.

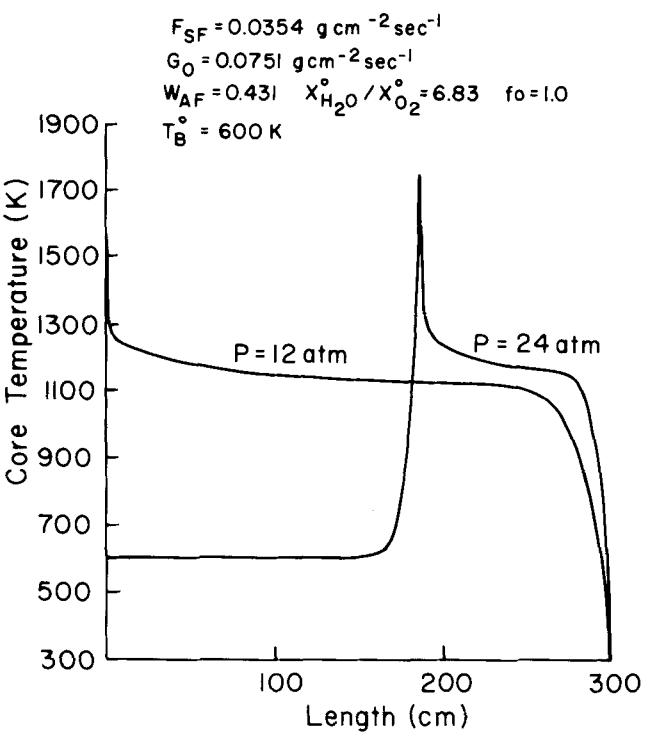

Fig. 17. Effect of changes in pressure on core temperature profiles.

Effect of Temperature Changes of Gaseous Feed Stream

Increases in the temperature of the gas fed to the bottom of the gasifier while producing a proportional increase in the maximum gas phase temperature practically does not

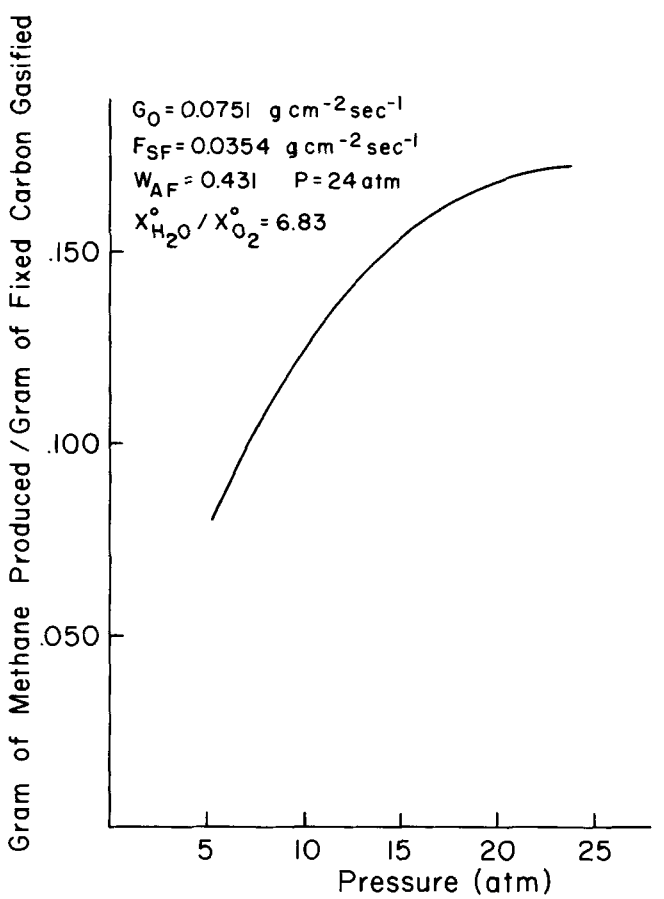

Fig. 18. Effect of changes in pressure on the amount of methane produced per unit mass of fixed carbon fed.

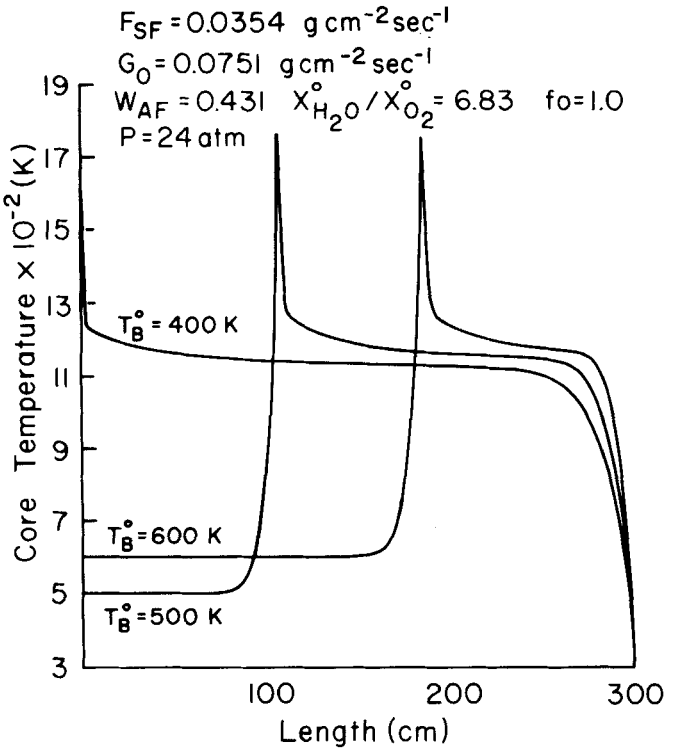

Fig. 19. Effect of changes in gaseous feed temperature on core temperature profiles.

affect the maximum core and solid external surface temperature, provided the total energy input is high enough to insure the complete gasification of the carbon fed to the reactor. If this last condition is not met and unreacted carbon leaves the gasifier, we have already shown that the maximum solid temperature occurs at the very bottom of the gasifier and decreases when the final carbon conversion does. Figure 19 shows the resulting core temperature profiles for three different inlet temperatures: 400°, 500°, and 600°K. All the other operating conditions were kept fixed and their values indicated on the graph. The already typical traveling of the oxygen consumption region can be seen. For $T_B^{\circ} = 400$°K, incomplete conversion is achieved. This increase in conversion without the accompanying increase in maximum core temperature (as was the case for increases in the steam/oxygen ratio) indicates the convenience of using the highest possible feed temperature, especially when we have to work dangerously close to the ash melting point.

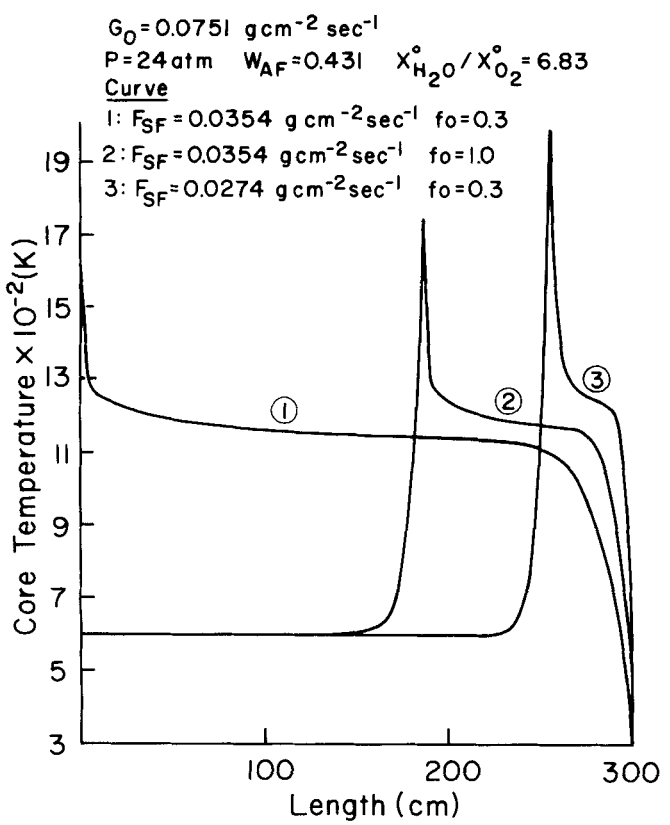

Fig. 20. Effect of changes in coal reactivity on core temperature profiles.

Coal Reactivity

We have characterized the coal reactivity by a reactivity factor f_o, whose value ranges from about 0.3 for anthracite to 10 or above for lignites. It is known that high reactivity coals produce a lower maximum temperature, and obviously a larger solid throughput can be completely gasified for otherwise identical operating conditions. This is precisely what can be seen in the core temperature profiles in Figure 20. Curves labeled 1 and 2 represent results for two different coals characterized by reactivity factors of 0.3 and 1.0. All the operating conditions are identical. Complete conversion is predicted for the higher reactivity coal, while only an 82.64% conversion is expected for $f_o = 0.3$. If, on the other hand, we reduce the solid mass flow rate for the lower reactivity coal in order to obtain complete conversion, curve 3 is obtained. The maximum temperature is now 240°K higher than that obtained under equivalent complete conversion for a coal with $f_o = 1.0$. We have already seen that the maximum temperature is independent of the C/O relation provided an ash layer is developed, and therefore such a high value is characteristic of a coal of a given reactivity factor.

NOTATION

(Quantities defined in the previous paper are not repeated here.)

a = interfacial area per unit bed volume
$\langle C_p \rangle$ = average specific heat of gas phase
$\tilde{C}_{pi}$ = specific heat of i^{th} component
F = solid mass flow rate
F_{SF} = fixed carbon plus ash mass flow rate at feed conditions
G = total mass flow rate of gas phase
g_i = moles of i^{th} component per unit mass of gas mixture
$\bar{h}_i$ = partial enthalpy per unit mass of i^{th} component
h_f = interfacial heat transfer coefficient
I = integral
K_R = apparent axial conductivity due to radiation
K_{WS} = water gas shift reaction equilibrium constant
L = reactor length
M_i = molecular weight of the i^{th} species
N_i = molar flow of the i^{th} species
P = reactor pressure
Q = total rate of carbon consumption per unit area of core surface
q_c = heat radiated and conducted from combustion zone to any point in the gasification zone in WLMG model
R = rate of carbon conversion due to steam gasification in moles of carbon gasified per unit particle volume
T_a = ambient temperature
T_{av} = average temperature in particle ash layer

T_o = maximum temperature to which char has been exposed previous to gasification in IGT kinetic scheme
T_p = particle temperature
T_{P2} = feed particle temperature
T_{PS} = solid external surface temperature
T_w = temperature of internal walls at the bottom of gasifier
t = time
w_{AF} = ash mass fraction in solid feed
w_i = mass fraction of i^{th} gaseous component
X^* = solid conversion at the transition between zones
x = axial coordinate in reactor
x^* = location of the transition between combustion and gasification zones
X_f = final conversion

Greek Letters

ΔH_i = enthalpy change for the i^{th} reaction
δ_H = ash-layer thickness whose resistance to heat transfer is equivalent to that of the film surrounding the particle
ϵ_b = bed porosity
ξ = sum of water and carbon dioxide concentrations
ρ_a = mass of ash per unit particle volume
ρ_c = mass of fixed carbon per unit particle volume
ρ_s = particle density
ρ_{SF} = particle density at feed

Subscript

B = condition in the bulk phase
c = condition at the core surface
1 = condition at the transition between gasification and combustion zone
2 = condition at the top of the reactor

Superscript

o = condition at the gas inlet
c = condition at the core surface

LITERATURE CITED

Arri, L. E., and Neal R. Amundson, "An Analytical Study of Single Particle Char Gasification," *AIChE J.*, (in press).

Beverage, G. S. G., and P. J. Goldie, "Analysis of Non-Isothermal Moving Beds for Non-Catalytic Solid-Gas Reactions," *Chem. Eng. Sci.*, **23**, 913 (1968).

Elgin, D. C., and H. R. Perks, "Trials of American Coals in a Lurgie Pressure Gasification Plant at Wesefield, Scotland," *I.G.T. Symposium Papers*, p. 127 (1973).

Elgin, D. C., "Results of Trials of American Coals in a Lurgi Pressure Gasification Plant at Westfield, Scotland," Proceedings of 6th Synthetic Pipeline Gas Symposium, p. 247 (1974).

Hebden, D., "High Pressure Gasification under Slagging Conditions," Proceedings of 7th Synthetic Pipeline Gas Symposium, p. 385 (1975).

Hoogendorn, J. C., "Gas From Coal with Lurgi Gasification at Sasol," *I.G.T. Symposium Papers*, p. 111 (1973).

Ishida, M., and C. Y. Wen, "Analysis of Non-Isothermal Moving Bed for Non-Catalytic Solid-Gas Reactions," *Ind. Eng. Chem. Process Design Develop.*, **10**, 164 (1971).

Johnson, J. L., "Kinetics of Bituminous Coal Char Gasification with Gases Containing Steam and Hydrogen," *Adv. in Chem. Ser. A.C.S.*, 131 (1974).

Rudolph, P., "Processing of American Coals in Lurgi Gasifier," Proceedings of 6th Synthetic Pipeline Gas Symposium, p. 269 (1974).

———, "The Lurgi Process. The Route to SNG From Coal," Proceedings of 4th Synthetic Pipeline Gas Symposium, p. 175 (1972).

Wen, C. Y., and S. C. Wang, "Thermal and Diffusional Effects in Non-Catalytic Solid-Gas Reactions," *Ind. Eng. Chem.*, **62**, No. 8, 30 (1970).

Woodmansee, D. E., "Modeling of Fixed Bed Gas Producer Performance," 5th Conference on Synthetic Fuels from Coal, Univ. Okla., Stillwater (May, 1975).

Yoon, H., James Wei, Morton M. Denn, "A Model for Moving Bed Coal Gasification Reactors," presented AIChE Annual Meeting, Chicago (1976).

Manuscript received June 29 and accepted August 23, 1977.

A Formulation for ϵ_M and ϵ_H Based on the Surface Renewal Principle

LINDON C. THOMAS

Department of Mechanical Engineering
University of Petroleum and Minerals
Dhahran, Saudi Arabia

This paper presents a simplified formulation for ϵ_H for low to moderate Prandtl number fluids and for ϵ_M that utilizes the surface renewal model, but which also accounts for the fact that eddies do not reach the surface. The predicted trend in Pr_t obtained on the basis of the present analysis suggests an opposite dependency on Pr to that predicted by many of the other analyses.

SCOPE

The primary objective of this paper is to demonstrate the relationship between the surface renewal approach to turbulence and the classical eddy diffusivity concept. The compatibility between these two approaches to turbulence has been previously demonstrated in the context of a comprehensive but complicated surface rejuvenation formulation. A simpler development is presented in this paper for moderate Prandtl numbers ($0.5 \lesssim Pr \lesssim 5.0$)

L. C. Thomas is presently on leave from the University of Akron, Akron, Ohio.